

# Oscillatory motion of a droplet in an active poroelastic two-phase model

Dirk Alexander Kulawiak<sup>1</sup>, Jakob Löber<sup>2</sup>, Markus Bär<sup>3</sup>,  
and Harald Engel<sup>1</sup>

<sup>1</sup> TU Berlin - Institut für Theoretische Physik, Hardenberstr. 36, 10623 Berlin, Germany; <sup>2</sup> Max-Planck-Institut für Physik komplexer Systeme, Nöthnitzer Straße 38, 01187 Dresden, Germany; <sup>3</sup> Physikalisch-Technische Bundesanstalt, Abbestrasse 2-12, 10587 Berlin, Germany

E-mail: [dirkk@itp.tu-berlin.de](mailto:dirkk@itp.tu-berlin.de)

December 2017

**Abstract.** We investigate flow-driven amoeboid motility as exhibited by microplasmodia of *Physarum polycephalum*. A poroelastic two-phase model with rigid boundaries is extended to the case of free boundaries and substrate friction. The cytoskeleton is modeled as an active viscoelastic solid permeated by a fluid phase describing the cytosol. A feedback loop between a chemical regulator, active mechanical deformations, and induced flows gives rise to oscillatory and irregular motion accompanied by spatio-temporal contraction patterns. We cover extended parameter regimes of active tension and substrate friction by numerical simulations in one spatial dimension and reproduce experimentally observed oscillation periods and amplitudes. In line with experiments, the model predicts alternating forward and backward ectoplasmatic flow at the boundaries with reversed flow in the center. However, for all cases of periodic and irregular motion, we observe practically no net motion. A simple theoretical argument shows that directed motion is not possible with a spatially independent substrate friction.

## 1. Introduction

Dynamic processes in cells, and cell motility in particular, are intriguing examples of large-scale spatio-temporal order in systems far from thermodynamic equilibrium [1, 2, 3]. Here, the continuous turnover of ATP by molecular motors [4] provides the energy to drive mechano-chemical contraction-expansion patterns and, ultimately, locomotion. Biological examples of these phenomena are reviewed and discussed in [5, 6, 7, 8].

A well-studied model organism exhibiting a huge variety of spatio-temporal mechano-chemical patterns with and without locomotion is the true slime-mold *Physarum polycephalum* [9, 10, 11]. *Physarum* is unicellular, but a cell contains multiple nuclei and can grow to the size of several square meters [12]. Microplasmodia are an artificial form of *Physarum* with a size between 100  $\mu\text{m}$  and 1 mm that do not occur in nature [13, 14, 15]. They are composed of a gel-like ectoplasm and a fluid-like endoplasm [16]. Microplasmodia are produced by extracting a sufficient amount of cytosol from a *Physarum* cell and placing it on a substrate. After reorganization, such a protoplasmic droplet displays a wide variety of spatio-temporal contraction patterns such as standing, traveling, and spiral waves as well as irregular oscillations [13]. After several hours, a cell elongates to a tadpole-like shape and starts to explore its surroundings [17, 18, 19, 20, 21]. In the remainder of this work, we use the terms microplasmodium and cell synonymously.

Movement of microplasmodia occurs in two modes: *peristaltic* and *amphistaltic* [16, 21]. In both modes microplasmodia alternate between forward and backward motion with a well defined period. The forward motion is larger than the backward motion, resulting in a net displacement within each period. In the more frequently observed peristaltic mode, motion is driven by mechano-chemical waves originating at the tail and traveling towards the front. In the amphistaltic mode, front and tail contract in anti-phase oscillations.

Common models for the cytoskeleton are based on active fluid and gel models [22, 23, 24, 25, 26]. In contrast, some models for the crawling type of amoeboid cell motility [27, 28] neglect intracellular flows. As opposed to simple fluids and solids, which are governed by a single momentum balance equation, poroelastic media belong to the class of two-fluid models. These are characterized by individual momentum balance equations for each of the constitutive phases. Such a description is useful if two phases with largely different rheological properties interpenetrate on relatively small length scales, such as groundwater permeating porous rock [29], the

superposition of normal and inviscid superfluid helium in helium II [30], or cytosol pervading the cytoskeleton.

Poroelastic two-phase models have been used to replicate the pattern formation in microplasmodia. Our work is based on the model introduced by Radszuweit et al. in [31, 32, 33, 34]. There, a feedback loop between an advected chemical regulator and active stress gives rise to spatio-temporal contraction patterns. The model can reproduce many experimentally observed contraction patterns in resting microplasmodia [13]. However, all earlier approaches studied resting microplasmodia with fixed boundaries. While this is simpler to implement in numerical simulations and allows to study intracellular deformations, it precludes the possibility of deformations of the cell boundary and motion of the cell as a whole. Here, we focus on cell motility which requires a non-trivial reformulation of the model and its boundary conditions.

## 2. Model

We model the cell's cytoplasm as a homogeneous [35, 36], isotropic [37], incompressible, and poroelastic medium [38, 39, 40]. The poroelastic material consists of two phases. The sponge-like cytoskeleton [25] is characterized as an active, viscoelastic solid with displacements  $u$  and velocity  $\dot{u}$ . The fluid phase representing the cytosol permeates the cytoskeleton and is described by a hydrodynamic flow velocity  $v$ . We use the terms gel for the solid cytoskeleton and fluid for the cytosol. Both phases individually satisfy a momentum balance equation expressed with stress tensors.  $\sigma_g$  and  $\sigma_f$  denote the stress in the gel and in the fluid, respectively. The total stress is given by  $\sigma = \rho_g \sigma_g + \rho_f \sigma_f$ , with  $\rho_g$  ( $\rho_f$ ) denoting the volume fraction of the gel (fluid) phase. We assume that the volume fractions are constant in time and space and satisfy  $\rho_g + \rho_f = 1$  [41]. A recent study has suggested that the activity difference between the two phases can lead to a phase separation [42]. A future extension of the presented model may include this phenomenon by treating the phase composition as a spatially dependent local variable.

A cell occupies a time dependent domain  $\mathcal{B}$  with boundaries denoted by  $\partial\mathcal{B}$ . Free boundary conditions enable the cell boundary to deform and move in response to bulk flow and deformation [43, 44, 45]. We assume that outside of the cell is an inviscid fluid described with stress tensor  $\sigma_{\text{out}} = -p_{\text{out}}$ . The exact value of the outside hydrostatic pressure  $p_{\text{out}}$  is not important, as long as it is constant and homogeneous. Thus, we choose  $p_{\text{out}} = 0$ . At the cell's boundary, the total stress has to be continuous across the interface.

This gives the first boundary condition

$$\sigma - p \Big|_{\partial\mathcal{B}} = \sigma_{\text{out}} \Big|_{\partial\mathcal{B}} = 0, \quad (1)$$

where the subscript  $\partial\mathcal{B}$  denotes evaluation at the boundary of domain  $\mathcal{B}$ . Because of the two momentum balance relations in the poroelastic model we need a second boundary condition. Assuming no polymerization of actin at, and no permeation of cytosol through the boundary, the velocity of gel and fluid must match. This gives rise to the boundary condition

$$\dot{u} \Big|_{\partial\mathcal{B}} = v \Big|_{\partial\mathcal{B}}. \quad (2)$$

Note that the free boundary conditions require the evaluation of stress tensors and flow fields at the boundary, whose position itself must be determined in the course of solving the evolution equations. We circumvent this problem by transforming the system to a co-moving frame of reference. In general, continuum mechanics allows to use different coordinate frames to formulate the model equations [46].

We distinguish between the lab frame (LF) with *spatial* coordinates  $X$  and the gel's body reference frame (BRF) with *material* coordinates  $x$ . The material displacement field  $u$  connects both frames by  $u(x, t) = X(x, t) - x$ . Note that a domain as well as its boundary which is time-dependent in the LF becomes stationary in the BRF. The gel velocity  $\dot{u}$  is given by the material time derivative  $\dot{u} = \partial_t u + (\partial_x u) \dot{x}$ . By definition, the gel is fixed in its BRF ( $\dot{x} = 0$ ) and the material time derivative simplifies to  $\dot{u} = \partial_t u$ . On the downside, transforming stress tensors given by linear constitutive laws from the LF to the BRF gives rise to many geometric nonlinearities. We simplify by linearizing in the strains, i.e., assuming  $|\partial_x u| \ll 1$ . However, note that we do not assume the displacements  $u$  to be small. The displacements may, for example, grow linearly in time without bounds for a cell moving with constant center of mass velocity. See [31, 32] for details on the transformation from the LF to the BRF, and Fig. 6 for a visual comparison of a quantity plotted in the BRF and the LF.

The fluid phase is modeled as a passive viscous liquid with stress  $\sigma_f = \eta_f v$ , where  $\eta_f$  is the viscosity. The stress  $\sigma_g = \sigma^{\text{ve}} + \sigma^{\text{act}}$  of the gel phase is decomposed in a passive part,  $\sigma^{\text{ve}}$ , and an active part,  $\sigma^{\text{act}}$ . We assume that the passive part is a viscoelastic Kelvin-Voigt solid with  $\sigma^{\text{ve}} = E \partial_x u + \eta_g \partial_x \dot{u}$  [47]. Here,  $E$  is Young's modulus and  $\eta_g$  the viscosity. Recently, the effects of alternative viscoelastic models for the passive gel stress were investigated in [48]. A poroelastic model with nonlinear elasticity was introduced in [49].

The active tension  $\sigma^{\text{act}} = T(c) = T_0 - \xi \frac{c}{1+c}$  is governed by the concentration  $c$  of a chemical regulator

species, which we assume to be calcium ions [25, 50].  $T_0$  is a homogeneous tension that is produced by motors in the cytoskeleton. These motors are inhibited by calcium that is dissolved in the fluid and advected with the fluid flow  $v$  in the LF. Furthermore, calcium diffuses with diffusion coefficient  $D_c$ . Transforming the advection-diffusion equation in the LF to the gel's BRF, and linearizing in the gel strains  $\partial_x u$ , yields an advection-diffusion equation with the relative velocity of the fluid to the gel  $v - \dot{u}$  as the advection velocity,

$$\partial_t c + \partial_x [(v - \dot{u}) c] = D_c \partial_{xx} c. \quad (3)$$

We assume that no calcium can cross the cell's membrane, resulting in a no-flux boundary condition for  $c$ . Thus, the total amount of calcium is conserved. Nevertheless, there can be local differences in the calcium concentration, which in turn drive mechanical deformations via a spatially varying activity  $T(c)$ . For a more detailed description of the intracellular calcium dynamics,  $c$  can be coupled to additional chemical species by chemical reactions as in [32, 34], but this aspect is neglected here.

Hence, we can write momentum balances in the BRF for both phases. The Reynolds numbers that arise from flows in the cytoplasm are small,  $\text{Re} \ll 1$ . Thus inertia effects can be neglected, and the cytoplasmic flow is described by the Stokes equation. The momentum balances read

$$\rho_g \partial_x (\sigma_g - p) + f_g + f_{\text{fric}} = 0, \quad (4)$$

$$\rho_f \partial_x (\sigma_f - p) + f_f = 0, \quad (5)$$

where  $p$  is the pressure stemming from the incompressibility of the medium expressed as

$$\partial_x (\rho_g \dot{u} + \rho_f v) = 0. \quad (6)$$

The friction between both phases is given by Darcy's law together with Newton's third law  $f_g = -f_f = \rho_g \rho_f \beta (v - \dot{u})$ . We assume a linear substrate friction force  $f_{\text{fric}} = -\rho_g \gamma \dot{u}$  for friction between gel and substrate, and no friction between fluid and substrate. In summary, the model equations are given by

$$\begin{aligned} \rho_f \eta_f \partial_{xx} v + \rho_g \eta_g \partial_{xx} \dot{u} + \rho_g E \partial_{xx} u \\ - \rho_g \gamma \dot{u} - \partial_x p &= -\rho_g \partial_x T(c) \end{aligned} \quad (7)$$

$$\eta_f \partial_{xx} v - \rho_g \beta (v - \dot{u}) - \partial_x p = 0 \quad (8)$$

$$\partial_x (\rho_g \dot{u} + \rho_f v) = 0. \quad (9)$$

$$\partial_t c + \partial_x [(v - \dot{u}) c] - D_c \partial_{xx} c = 0. \quad (10)$$

Note that the only nonlinear terms are the advection term for calcium and the active tension term  $T(c)$ . We introduce the dimension-less Péclet number  $\text{Pe} = \xi / (D_c \beta)$  as a measure for the ratio of diffusive to advective time scales to characterize the strength of the active tension [31].

### 3. Results

Equations 7-10 are solved with parameter values adopted from [31] and listed in Tab. 1 unless stated otherwise. The initial condition is the weakly perturbed homogeneous steady state (HSS) with  $u = \dot{u} = v = 0$  and  $c = c_0 = 1$ . Due to the incompressibility of the medium (Eq. 6), the cell's length  $L$  is constant. The location of the cell's left boundary is used as a measure of the cell's position. We observe a variety of spatio-temporal contraction patterns together with or without movement. Depending on parameter values, the cell's position over time remains fixed or undergoes regular or irregular oscillations. However, in all cases the temporal average of the cell's position vanishes, i.e. there is no net motion. To visualize the intracellular dynamics of calcium and gel flow we show space-time plots of these quantities in the BRF.

#### Symmetric and antisymmetric calcium oscillations

The case of a regular oscillations in Fig. 1 exemplifies how the different parts of the model interact and motion arises. Shortly after initialization, the concentration oscillates in a spatially symmetric manner with period  $T_{\text{sym}} = 24\text{s}$  (Fig. 1, top) and a constant position of the cell (Fig. 1, bottom). The blue lines in Fig. 2 show snapshots of the calcium concentration as a function of space. The calcium distribution changes periodically from a high concentration at the center and low values at the boundaries (top left panel) to a low concentration at the center and high values at the boundaries (bottom left panel). In the top left panel the active tension  $\partial_x T \sim \partial_x c$  (red line) generates a symmetric advection flow from the boundaries towards the center (black arrows). This results in even more calcium piling up at the center, thus causing an even stronger flow. The flow deforms the cell and elastic tension in the gel builds up. Over time, this elastic tension increases and acts in opposition to the active tension. The advection of calcium weakens, and at some point calcium diffusion takes over. The calcium concentration at the center starts to decrease, diminishing active tension and thereby advection even further. When the elastic tension overcomes the active tension the direction of advection changes. The concentration starts to pile up at the boundaries (bottom left panel), and the process repeats. During the whole oscillation cycle both the flow of the gel  $\dot{u}$  and the fluid  $v$  are symmetric in space. Hence, spatially symmetric oscillations result in immobile cells.

At  $t \approx 1800\text{s}$  in Fig. 1 a transition from symmetric to antisymmetric calcium oscillations occurs. Here, the calcium concentration is high at one boundary but low at the other. With increasing amplitude

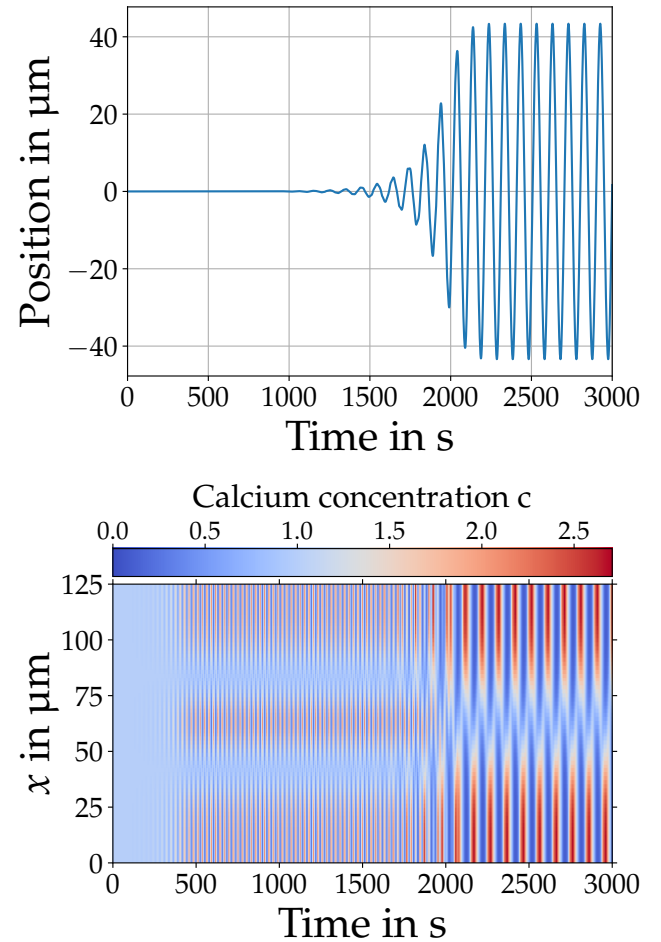


**Figure 1.** Regular oscillations of the cell's position over time (top) are accompanied by spatially antisymmetric calcium oscillations (bottom). The active tension ( $\text{Pe} = 6$ ) is slightly above the critical value where the HSS destabilizes. After initialization, the resting cell exhibits spatially symmetric calcium oscillations with period  $T_{\text{sym}} = 24\text{s}$  and slowly growing amplitude. After  $\approx 2000\text{s}$  a transition to spatially antisymmetric calcium oscillations occurs. Simultaneously the cell's position starts to oscillate with an amplitude of about  $1/3$  its length and a period  $T_{\text{antisym}} = 98\text{s}$ . The calcium concentration is plotted in a body reference frame co-moving with the gel phase.

of the antisymmetric oscillation, the cell starts to move periodically back and forth. After a transition period of  $\approx 200\text{s}$ , the amplitude of calcium oscillations saturates, and the cell performs periodic motion in phase with the calcium oscillations and a period of  $T_{\text{antisym}} = 98\text{s}$ . Fig. 2 (right) shows two snapshots of antisymmetric oscillations at different times. When the cell's position is at its maximum displacement to the right, the calcium concentration changes from having its maximum at the right boundary to being higher on the left boundary. When the maximum of the concentration switches sides, the active tension changes sign, causing an advective flow to the left. A

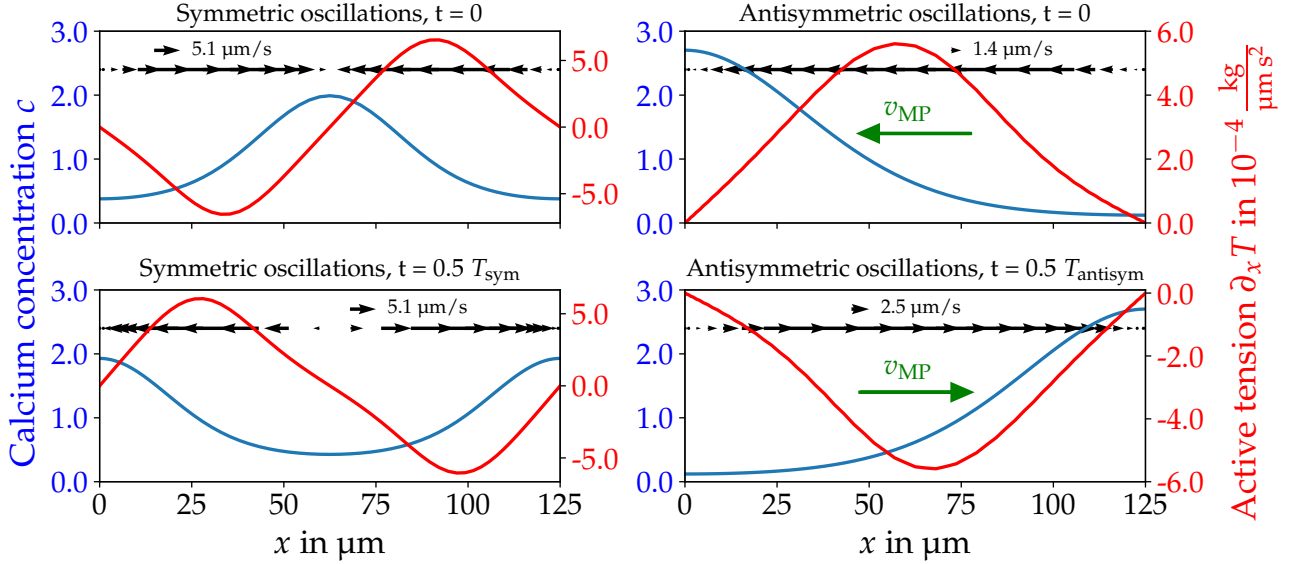


**Figure 2.** Snapshots of spatially symmetric (left) and antisymmetric (right) calcium oscillations. The calcium concentration  $c$  is depicted in blue, the active tension  $\partial_x T \sim \partial_x c$  in red, and black arrows indicate the advection velocity  $v = \dot{u}$ . The length of the black arrows indicates the amplitude of the advective flow. Spatially symmetric oscillations have a period of  $T_{\text{sym}} = 24$  s and  $c$  oscillates between high concentration at the center (top left) and high concentration at the boundaries (bottom left). No movement occurs. In the second case,  $c$  oscillates between two configurations antisymmetric to each other with a period of  $T_{\text{antisym}} = 98$  s (right). The cell is moving with velocity  $v_{\text{MP}}$  towards the direction of high calcium concentration as indicated by the green arrows.

rapid movement to the left starts with a maximum cell velocity of  $v_{\text{MP}} = 2.47$  μm/s. While this movement takes place, the concentration piles up on the left boundary (top right) and the elastic tension inside the cell builds up. Similar to the symmetric case, this elastic tension is acting in opposition to the active tension yielding a lower advection and cell velocity. At some point, advection becomes weaker than diffusion. Then, the concentration has reached its maximum and begins to decrease. While the active tension is diminishing, the elastic stress inside the gel phase still builds up. Once it overcomes the active tension, the tension in the cell starts to decay. This causes a change of direction of the advective flow, leading to a rise of concentration on the right, and the process repeats (bottom right). This antisymmetric oscillation results in a periodic cell movement with a maximum displacement of  $u_{\text{max}} \approx 42$  μm but not in net motion.

Depending on the value of the substrate friction strength  $\gamma$ , symmetric or antisymmetric calcium oscillations may occur. If  $\gamma \leq 7 \times 10^{-7}$  kg/s, the concentration exhibits symmetric oscillations comparable to the initial phase of Fig. 1 without motility. At  $\gamma_{\text{cr}} = 8 \times 10^{-7}$  kg/s, a transition to oscillatory motion accompanied by antisymmetric calcium oscillations takes place. If  $\gamma$  is above  $10^{-4}$  kg/s, the friction is too strong to permit pattern formation. The HSS is stable, and small perturbations decay.

#### Varying the active tension strength excites different modes of motion

Depending on the strength of the active tension as measured by the dimensionless Péclet number  $\text{Pe}$ , the cell's position is stationary or oscillates with one or many frequencies. We decompose the position over time data in frequency components and use the number of excited Fourier modes  $\theta$  to characterize the periodic movement. Fig. 3 gives an overview how  $\theta$  develops when changing  $\text{Pe}$ .

In agreement with the linear stability analysis from [31], for very low values of  $\text{Pe} < 5.75$  the active tension is not strong enough to destabilize the HSS, and small perturbations relax back to the HSS. Increasing  $\text{Pe}$  beyond 5.75 destabilizes the HSS by a Hopf-bifurcation and the cell's position exhibits regular oscillations together with antisymmetric calcium oscillations. A further increase yields a regime without motion ( $\theta = 0$ ). Although the HSS is unstable in this regime the cell does not move because the calcium undergoes spatially symmetric oscillations. In contrast to the case of transient symmetric oscillations in Fig. 1, here the symmetric oscillations remain stable on the timescale of the simulation length (at least 10000 s).

If  $\text{Pe} \geq 7.4$ , a sudden transition to  $\theta = 4$  occurs and the cell moves again. The number of excited Fourier modes  $\theta$  rises fast with a further increase of  $\text{Pe}$ . The motion of the cell becomes irregular and the

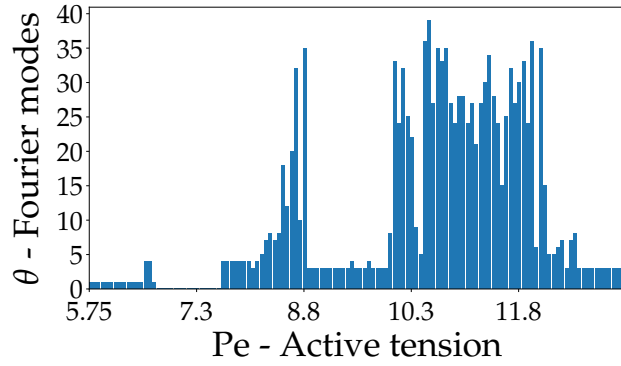


Figure 3. Number of excited Fourier modes  $\theta$  in the position over time data for different strengths of active tension  $\xi$  as measured by the dimensionless Péclet number  $\text{Pe} = \xi/(D_c\beta)$ . For low values ( $\text{Pe} < 5.75$ ) the HSS is stable. Increasing  $\text{Pe} \geq 5.75$  destabilizes the HSS by a Hopf-bifurcation and cells exhibit regular oscillations. A further increases yields resting cells with symmetric calcium oscillations ( $6.6 < \text{Pe} < 7.4$ ) and regimes with cells exhibiting irregular motion (e.g.  $9.25 < \text{Pe} < 11.5$ ).

spectrum of its trajectory is continuous. A maximum is reached at  $\text{Pe} = 8.3$  with  $\theta = 35$  modes. An example of an irregular oscillation with  $\text{Pe} = 8.35$  is shown in Fig. 4. Between  $\text{Pe} = 8.45$  and  $\text{Pe} = 9.2$ , the number of Fourier modes stays constant with  $\theta = 3$  and a fundamental period of  $\approx 94$  s. Beginning with  $\text{Pe} = 9.25$ , the movement becomes irregular again. In this regime up to  $\theta = 38$  modes can be observed and the motion is again comparable to the one displayed in Fig. 4. Upwards from  $\text{Pe} = 11.5$  the cell oscillates with  $\theta = 3$ . The amplitude of the fundamental mode with a period of about 25 s is much larger than the other ones. Thus, the movement is quasi-regular but with a higher frequency than in Fig. 1.

#### Comparison with experiments

In experiments, directed motion of cells is accompanied by oscillations with a period between 85 s and 110 s. During the peristaltic mode of motion, cells undergo a forward displacement of  $d_F \approx 40$   $\mu\text{m}$ , followed by a backward displacement of  $d_B \approx 15$   $\mu\text{m}$ -20  $\mu\text{m}$  [21, 16]. As displayed in Fig. 3, we find regular oscillations for large parameter regimes in our simulations. As shown in Fig. 1, once the dominant pattern with regular, antisymmetric calcium oscillations has emerged, the cell's position over time oscillates with a period of  $T = 98$  s and undergoes displacements of  $d \approx 82$   $\mu\text{m}$ . However, we always find  $d = d_F = d_B$  such that no net motion occurs.

Additionally, we compare experimentally observed flow patterns within the cell with simulations. The space-time plot in Fig. 5 compares the gel flow (top) with experimentally obtained ectoplasmic flow

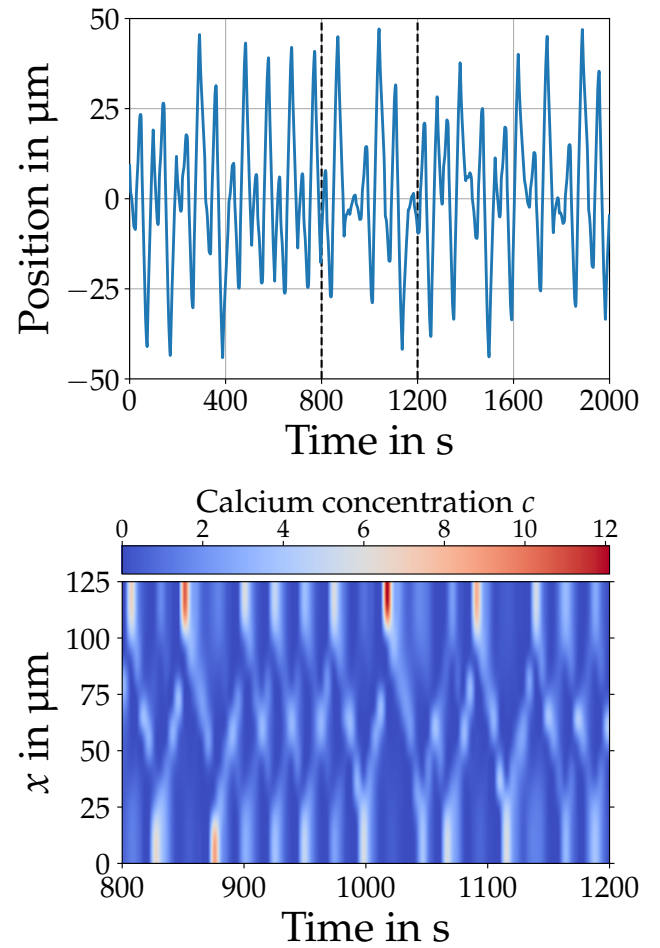
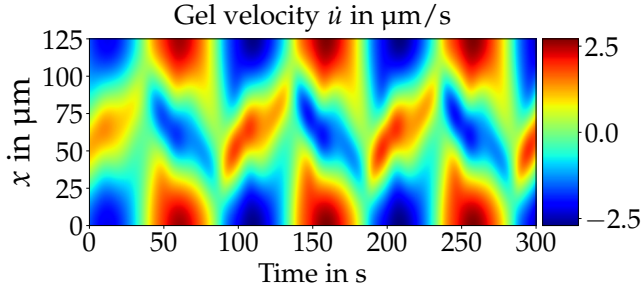


Figure 4. Irregular oscillations of the cell's position over time (top) appear together with asymmetric calcium profiles (bottom). With an active tension ( $\text{Pe} = 8.35$ ) higher than in Fig. 1 the cell's movement and calcium dynamics becomes irregular. However, averages of the cell's position over long times still vanish such that there is no net motion.

(bottom) for the peristaltic mode of motion from [16]. At a fixed position, the flow alternates periodically between forward and backward flow. While the flow directions at front and back are equal, with a higher magnitude at the back, the center part is flowing towards the opposite direction with weaker magnitude than flow at the boundaries. Experimentally, flows towards the front have a larger magnitude than backward flows, resulting in a net propagation velocity of the entire cell of  $v_{\text{exp}} \approx 0.15$ -0.2  $\mu\text{m/s}$ . In simulations, forward and backward flows have equal magnitude and thus cancel within one oscillation period.

Spatio-temporal measurements of calcium ( $\text{Ca}^{2+}$ ) dynamics reveal that cell motility is accompanied by calcium wave patterns. These resemble traveling waves in the peristaltic mode and standing waves in the amphistaltic mode [16]. The cells in our simulations never exhibit net motion and we observe only standing



**Figure 5. Gel velocity in simulation for a regular oscillation.** At a fixed position, the flow direction alternates between forward and backward with a period of about 100s in experiment [16] as well as in simulation. Flow at the center is opposite and of weaker magnitude than flow at the boundaries. Experimental backward flow is of weaker magnitude than the forward flow, resulting in a net motion. Simulated forward and backward flows have equal magnitude and thus cancel exactly. An experimental flow profile is shown in [16], Fig 7.

or irregular wave patterns. Note, however, that we model calcium dynamics in form of an advection-diffusion equation whereas in experimental systems, calcium additionally takes part in chemical reactions [34, 51].

#### 4. Discussion

To model motile cells, continuum mechanical models must be supplemented with free boundary conditions. Here we extended the poroelastic model with rigid boundaries from [31, 32, 33, 34] to the case of free boundaries and included linear friction with the substrate to study motile *Physarum* microplasmidia. We observed different modes of motion ranging from resting cells to cells performing regular and irregular oscillations. We covered extended parameter regimes by simulation and identified parameters that reproduce experimentally observed oscillation periods of about 100s. Additionally, as shown in Fig. 5, the simulated flow patterns resemble experimentally measured flow patterns.

The question arises why, for all cases of periodic and even irregular motion, the time averaged position vanishes, and no net motion occurs. A simple calculation shows that net motion is impossible for a substrate friction  $\gamma$  constant in space. For constant mass density, the velocity  $\bar{v}$  of the cell's center of mass is obtained by spatially averaging the gel velocity

$$\bar{v} = \frac{1}{V_0} \int_{\mathcal{B}} u dx, \quad (11)$$

with  $V_0$  the constant volume of the cell (length in one spatial dimension). Adding the force balances for gel and fluid phase, Eq. 4 and Eq. 5, yields

$$\bar{v} = \frac{1}{V_0} \int_{\mathcal{B}} \frac{1}{\gamma} \partial_x (\sigma - p) dx. \quad (12)$$

For  $\gamma$  constant in space, we may use Gauss theorem to transform the volume integral to a surface integral with normal vector  $n$ ,

$$\bar{v} = \frac{1}{\gamma V_0} \oint_{\partial \mathcal{B}} (\sigma - p) n dS. \quad (13)$$

Together with the free boundary condition Eq. 1, we immediately obtain a vanishing center of mass velocity  $\bar{v} = 0$ . This is confirmed by a direct calculation of  $\bar{v}$  in numerical simulations as given by Eq. 11.

Thus a spatially dependent substrate friction seems to be an essential ingredient to obtain net motion. This is in line with the results from [21], where a space-dependent friction coefficient was introduced and net motion was observed. In addition, the authors in [16] found evidence for a nonlinear relationship between cell velocity and traction force yielding a position-dependent friction coefficient.

Another essential ingredient to achieve directed motion is a mechanism which breaks the front-back symmetry and thus establishes a polarity [52]. The calcium distributions produced by the pure diffusion-advection dynamics chosen for this model may look asymmetric at certain instants in time, but the time averaged distribution is always symmetric. If that is a reason for or a consequence of the fact that we do not observe net motion remains to be investigated. In [21, 53] the breaking of the front-back symmetry was realized by externally forcing friction coefficient and contractile stress in form of a traveling wave. A self-organized way to break the spatial symmetry and introduce a polarity in the cell is to include a reaction kinetics for calcium as done in [32, 34].

With minor modifications, our model might be applicable to other systems. We highlight photosensitive self-oscillating gels where the swelling is regulated by an embedded, light-sensitive chemical reaction [54, 55, 56, 57]. Applying appropriate illumination pattern generates directed waves of a regulator which lead to oscillatory motion of the gel with [54] and without [56] net motion. Some parameters in this chemical reaction are easier to control experimentally than in *Physarum* microplasmidia. Therefore, it could be a helpful setup to study the transition from motion without to motion with net motion.

#### 5. Numerical Details

We solve the equations of motion on an one-dimensional Chebyshev-Lobatto grid [58] of size  $L$  with  $N$  points. We utilize no-flux boundary conditions for the concentrations  $c$  and free boundary conditions for the mechanical equations. We formulate our model in the gel's body reference frame (BRF). For details about the derivation of the model refer to [32, 34]

We split the full equations from Eq. 7 - Eq. 10 into a mechanical and an advection-diffusion part and solve each part separately. We use pseudo-spectral methods (Chebyshev) for the discretized spatial derivatives and the Euler method for time-stepping.

For the mechanical part, we introduce  $U \equiv \partial_t u = \frac{u - u^t}{\Delta t}$ , where  $t$  denotes the current time-step and variables without explicit time dependency are at time  $t + \Delta t$ . Then, we arrive at

$$u - U\Delta t = u^t \quad (14)$$

$$\rho_f \eta_f \partial_{xx} v + \rho_g \eta_g \partial_{xx} U + \rho_g E \partial_{xx}$$

$$u - \gamma \rho_g U - \partial_x p = -\rho_g \partial_x T(c^t) \quad (15)$$

$$\eta_f \partial_{xx} v - \rho_g \beta(v - U) - \partial_x p = 0 \quad (16)$$

$$\partial_x(\rho_g U + \rho_f v) = 0. \quad (17)$$

Then, we solve the advection-diffusion part semi-implicitly with  $\partial_t c = \frac{c - c^t}{\Delta t}$ . This approach yields

$$c + \Delta t \partial_x(w^t) - \Delta t D_c \partial_{xx} c = c^t, \quad (18)$$

where  $w = v - U$  is the fluid velocity in the gel's BRF. This yields the linear equation

$$(1 - \Delta t D_c \partial_{xx} + \Delta t \partial_x w^t) c = c^t. \quad (19)$$

We solve our equations using python [59] with the iterative gmres solver from scipy and an ILU preconditioner.

## 6. Calcium Concentration in Body Reference and Lab Frame

We solve our model equations in the gel's BRF and the resulting quantities are defined in this frame. However, we as observers are located in the lab frame (LF). Fig. 6 shows how a regular calcium oscillation (compare with Fig. 1 in the main text) looks in BRF as well as LF. The transformation of quantities from the BRF to the LF is given by the deformation field  $u$  with  $X_0 = x_0 + u(x_0)$ , where  $x_0$  the position in the BRF and  $X_0$  is the position in the LF.

The concentration in Fig. 6 exhibits spatially antisymmetric oscillations in the BRF and switches between a state with a high value of calcium at the left boundary and a low value at the right boundary and the reversed state. In the LF, this yields a periodic movement of the cell. As long as the concentration has a local maximum at a certain boundary the cell is moving into this direction.

## 7. Parameters

## 8. Acknowledgments

We thank Markus Radszuweit for helpful discussions about his previous work on the model. Computational

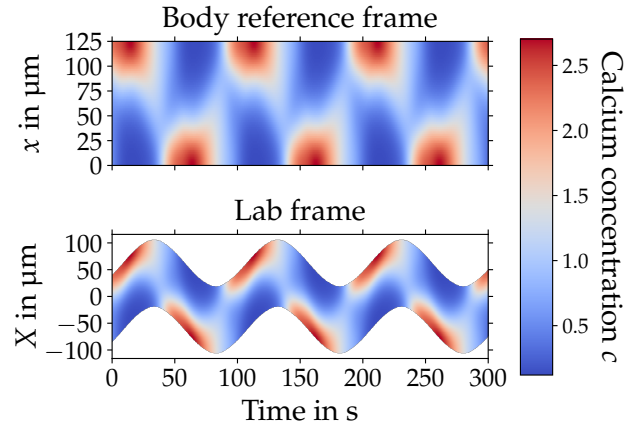


**Figure 6.** Spatially antisymmetric calcium oscillation in body reference (top) and lab frame (LF) (bottom). In the LF, the cell is moving into the direction where  $c$  has a local maximum. The regular calcium oscillation yields a periodic movement with a period of 98 s.

**Table 1. Physarum parameters**

Par	Description	Value	Units
$N$	Number of grid points	120	-
$\Delta t$	Numerical time step	0.001	s
$D_c$	Calcium diffusion	200	$\mu\text{m}^2 \text{s}^{-1}$
$L$	Length	125	$\mu\text{m}$
$\rho_g$	Gel fraction	0.5	-
$\rho_f$	Fluid fraction	0.5	-
$\eta_g$	Viscosity gel	$10^{-2}$	$\frac{\text{kg}}{\mu\text{m} \text{s}}$
$\eta_f$	Viscosity fluid	$2 \times 10^{-8}$	$\frac{\text{kg}}{\mu\text{m} \text{s}}$
$\beta$	Friction between both phases	$10^{-4}$	$\frac{\text{kg}}{\mu\text{m}^3 \text{s}}$
$E$	Young modulus	0.01	$\frac{\text{kg}}{\mu\text{m}^2}$
Pe	Active tension	6	-
$\gamma$	Substrate friction	$10^{-5}$	$\text{kg s}^{-1}$

These parameters are used throughout this work any derivation is explicitly marked, taken from [31].

resources were provided by the Institut für Theoretische Physik at the TU Berlin. DAK was funded by the German Science Foundation (DFG) within the GRK 1558.

## 9. References

- [1] Murray J D 2007 *Mathematical Biology 1: An Introduction* 3rd ed (Springer) ISBN 978-0-387-22437-4 URL <https://www.springer.com/us/book/9780387952239>
- [2] Winfree A T 2001 *The Geometry of Biological Time* (New York, NY: Springer New York) ISBN 978-0-387-98992-1 URL <http://link.springer.com/10.1007/978-1-4757-3484-3>
- [3] Prigogine I 1978 *Science* 777–785 URL <http://www.jstor.org/stable/1746122>
- [4] Kolomeisky A B and Fisher M E 2007 *Annual Re-*

view of Physical Chemistry **58** 675–695 URL <http://www.annualreviews.org/doi/10.1146/annurev.physchem.58.032806.104532>

[5] Gross P, Kumar K V and Grill S W 2017 *Annual Review of Biophysics* **46** 337–356 ISSN 1936-122X, 1936-1238 URL <http://www.annualreviews.org/doi/10.1146/annurev-biophys-070816-033602>

[6] Nishikawa M, Naganathan S R, Jülicher F and Grill S W 2017 *eLife* URL <https://elifesciences.org/articles/19595>

[7] Howard J, Grill S W and Bois J S 2011 *Nature Reviews Molecular Cell Biology* **12** 392–398 URL <https://www.nature.com/nrm/journal/v12/n6/abs/nrm3120.html>

[8] Mayer M, Depken M, Bois J S, Jülicher F and Grill S W 2010 *Nature* **467** 617–621 ISSN 0028-0836, 1476-4687 URL <http://www.nature.com/doifinder/10.1038/nature09376>

[9] Oettmeier C, Brix K and Doeberleiner H G 2017 *Journal of Physics D: Applied Physics* URL <http://iopscience.iop.org/article/10.1088/1361-6463/aa8699>

[10] Aldrich H C and Daniel J W (eds) 1982 *Cell Biology of Physarum and Didymium* (New York: Academic Press) ISBN 978-0-12-049601-3 URL <https://www.sciencedirect.com/science/book/9780120496013>

[11] Teplov V A 2017 *Journal of Physics D: Applied Physics* **50** ISSN 0022-3727, 1361-6463 URL <http://iopscience.iop.org/article/10.1088/1361-6463/aa6727/meta>

[12] Fessel A, Oettmeier C and Doeberleiner H G 2015 *Nano Communication Networks* **6** 87–95 URL [www.sciencedirect.com/science/article/pii/S1878778915000174](http://www.sciencedirect.com/science/article/pii/S1878778915000174)

[13] Takagi S and Ueda T 2008 *Physica D: Nonlinear Phenomena* **237** 420–427 URL <http://www.sciencedirect.com/science/article/pii/S0167278907003417>

[14] Takagi S and Ueda T 2010 *Physica D: Nonlinear Phenomena* **239** 873–878 URL [www.sciencedirect.com/science/article/pii/S0167278909002103](http://www.sciencedirect.com/science/article/pii/S0167278909002103)

[15] Bernitt E, Oettmeier C and Doeberleiner H G 2010 Microplasmodium dynamics of Physarum polycephalum 6th World Congress of Biomechanics (Springer) pp 1133–1136 URL <http://www.springerlink.com/index/X532906434242217.pdf>

[16] Zhang S, Guy R, Lasheras J C and del Álamo J C 2017 *Journal of Physics D: Applied Physics* URL <http://iopscience.iop.org/article/10.1088/1361-6463/aa68be/meta>

[17] Matsumoto K, Takagi S and Nakagaki T 2008 *Biophysical Journal* **94** 2492–2504 ISSN 00063495 URL <http://linkinghub.elsevier.com/retrieve/pii/S0006349508705058>

[18] Rieu J P, Delanoe-Ayari H, Takagi S, Tanaka Y and Nakagaki T 2015 *Journal of The Royal Society Interface* **12** URL <http://rsif.royalsocietypublishing.org/cgi/doi/10.1098/rsif.2015.0099>

[19] Rodiek B and Hauser M J B 2015 *The European Physical Journal Special Topics* **224** 1199–1214 URL <http://link.springer.com/10.1140/epjst/e2015-02455-2>

[20] Rodiek B, Takagi S, Ueda T and Hauser M J B 2015 *European Biophysics Journal* **44** 349–358 URL <http://link.springer.com/10.1007/s00249-015-1028-7>

[21] Lewis O L, Zhang S, Guy R D and del Alamo J C 2015 *Journal of The Royal Society Interface* **12** URL <http://rsif.royalsocietypublishing.org/cgi/doi/10.1098/rsif.2014.1359>

[22] Jülicher F, Kruse K, Prost J F and Joanny J 2007 *Physics Reports* **449** 3–28 URL <http://www.sciencedirect.com/science/article/pii/S0370157307001330>

[23] Joanny J F and Prost J 2009 *HFSP Journal* **3** 94–104 URL <http://www.tandfonline.com/doi/abs/10.2976/1.3054712>

[24] Köpf M and Pismen L M 2013 *Physica D: Nonlinear Phenomena* **259** 48–54 ISSN 01672789 URL <http://linkinghub.elsevier.com/retrieve/pii/S0167278913001577>

[25] Bois J S, Jülicher F and Grill S W 2011 *Physical Review Letters* **106** URL <http://link.aps.org/doi/10.1103/PhysRevLett.106.028103>

[26] Strychalski W, Copos C A, Lewis O L and Guy R D 2015 *Journal of Computational Physics* **282** 77–97 URL <http://linkinghub.elsevier.com/retrieve/pii/S0021999114006780>

[27] Kulawiak D A, Camley B A and Rappel W J 2016 *PLOS Computational Biology* **12** URL <http://dx.plos.org/10.1371/journal.pcbi.1005239>

[28] Löber J, Ziebert F and Aranson I S 2014 *Soft Matter* **10** 1365–1373 URL <http://xlink.rsc.org/?DOI=C3SM51597D>

[29] Coussy O 2004 *Poromechanics* 2nd ed (Chichester, England ; Hoboken, NJ: Wiley) ISBN 978-0-470-84920-0 URL <https://www.wiley.com/en-us/Poromechanics-p-9780470849200>

[30] Landau L D and Lifschitz E M 1987 *Fluid Mechanics* 2nd ed (Oxford, England ; New York: Pergamon Press) ISBN 978-0-08-033933-7 URL <https://www.sciencedirect.com/science/book/9780080339337>

[31] Radszuweit M, Alonso S, Engel H and Bär M 2013 *Physical Review Letters* **110** URL <http://link.aps.org/doi/10.1103/PhysRevLett.110.138102>

[32] Radszuweit M, Engel H and Bär M 2014 *PLoS ONE* **9** URL <http://dx.plos.org/10.1371/journal.pone.0099220>

[33] Radszuweit M, Engel H and Bär M 2010 *The European Physical Journal Special Topics* **191** 159–172 URL <http://www.springerlink.com/index/10.1140/epjst/e2010-01348-2>

[34] Alonso S, Strachauer U, Radszuweit M, Bär M and Hauser M J 2016 *Physica D: Nonlinear Phenomena* **318** 58–69 URL <http://www.sciencedirect.com/science/article/pii/S0167278915001906>

[35] Nagai R and Kato T 1975 *Protoplasma* **86** 141–158 URL <http://link.springer.com/article/10.1007/BF01275628>

[36] Isenberg G and Wohlfarth-Bottermann K E 1976 *Cell and tissue research* **173** 495–528 URL <http://www.springerlink.com/index/w47u0183401859qm.pdf>

[37] Brix K, Kukulies J and Stockem W 1987 *Protoplasma* **137** 156–167 URL <http://link.springer.com/article/10.1007/BF01281151>

[38] Alt W and Dembo M 1999 *Mathematical Biosciences* **156** 207–228 URL <http://www.sciencedirect.com/science/article/pii/S0025556498100676>

[39] Joanny J F, Jülicher F, Kruse K and Prost J F 2007 *New Journal of Physics* **9** 422–422 URL <http://iopscience.iop.org/article/10.1088/1367-2630/9/11/422/meta>

[40] Oster G F and Odell G M 1984 *Physica D: Nonlinear Phenomena* **12** 333–350 URL <http://www.sciencedirect.com/science/article/pii/0167278984905372>

[41] Dembo M and Harlow F 1986 *Biophysical Journal* **50** 109–121 URL [http://www.cell.com/biophysj/pdf/S0006-3495\(86\)83444-0.pdf](http://www.cell.com/biophysj/pdf/S0006-3495(86)83444-0.pdf)

[42] Weber C, Rycroft C H and Mahadevan L 2017 *arXiv preprint arXiv:1710.03633* URL <https://arxiv.org/abs/1710.03633>

[43] Larripa K and Mogilner A 2006 *Physica A: Statistical Mechanics and its Applications* **372** 113–123 URL <http://www.sciencedirect.com/science/article/pii/S0378437106005905>

[44] Nickaeen M, Novak I L, Pulford S, Rumack A, Brandon J, Slepchenko B M and Mogilner A 2017 *PLOS Computational Biology* **13** URL <http://dx.plos.org/10.1371/journal.pcbi.1005862>

[45] Köpf M H and Pismen L M 2013 *Soft Matter* **9** 3727–3734 URL <http://pubs.rsc.org/-/content/>

articlelanding/2013/sm/c3sm26955h

- [46] Chaves E W V 2013 *Notes on Continuum Mechanics* 1st ed (Springer Netherlands) ISBN 978-94-007-5986-2 URL <https://www.springer.com/de/book/9789400759855>
- [47] Banks H T, Hu S and Kenz Z R 2011 *Advances in Applied Mathematics and Mechanics* **3** 1–51 URL [http://journals.cambridge.org/abstract\\_S207007330000151X](http://journals.cambridge.org/abstract_S207007330000151X)
- [48] Alonso S, Radszuweit M, Engel H and Bär M 2017 *Journal of Physics D: Applied Physics* **50** URL <http://iopscience.iop.org/article/10.1088/1361-6463/aa8a1d>
- [49] Taber L, Shi Y, Yang L and Bayly P 2011 *Journal of mechanics of materials and structures* **6** 569–589 URL <https://msp.org/jomms/2011/6-1/p35.xhtml>
- [50] Yoshimoto Y, Matsumura F and Kamiya N 1981 *Cytoskeleton* **1** 433–443 URL <http://onlinelibrary.wiley.com/doi/10.1002/cm.970010404/full>
- [51] Dupont G, Falcke M, Kirk V and Sneyd J 2016 *Models of Calcium Signalling* (Cham: Springer International Publishing) ISBN 978-3-319-29645-6 URL <http://link.springer.com/10.1007/978-3-319-29647-0>
- [52] Rappel W J and Edelstein-Keshet L 2017 *Current Opinion in Systems Biology* 43–53 URL <http://www.sciencedirect.com/science/article/pii/S2452310016300166>
- [53] Lewis O L and Guy R D 2017 *Journal of Physics D: Applied Physics* **50** URL <http://iopscience.iop.org/article/10.1088/1361-6463/aa76c3/meta>
- [54] Lu X, Ren L, Gao Q, Zhao Y, Wang S, Yang J and Epstein I R 2013 *Chemical Communications* **49** 7690–7692 URL <http://xlink.rsc.org/?DOI=c3cc44480e>
- [55] Ren L, She W, Gao Q, Pan C, Ji C and Epstein I R 2016 *Angewandte Chemie International Edition* **55** 14301–14305 URL <http://doi.wiley.com/10.1002/anie.201608367>
- [56] Ren L, Wang M, Pan C, Gao Q, Liu Y and Epstein I R 2017 *Proceedings of the National Academy of Sciences* **114** 8704–8709 URL <http://www.pnas.org/content/114/33/8704>
- [57] Epstein I R and Gao Q 2017 *Chemistry - A European Journal* **23** 11181–11188 ISSN 09476539 URL <http://doi.wiley.com/10.1002/chem.201700725>
- [58] Trefethen L N 2000 *Spectral Methods in MATLAB* (SIAM) ISBN 978-0-89871-465-4
- [59] Oliphant T E 2007 *Computing in Science & Engineering* **9** 10–20 ISSN 1521-9615 URL <http://ieeexplore.ieee.org/document/4160250/>